SolarPACES 2023, 29th International Conference on Concentrating Solar Power, Thermal, and Chemical Energy Systems

Receivers and Heat Transfer Media and Transport: Point Focus Systems

https://doi.org/10.52825/solarpaces.v2i.899

Published: 01 Aug. 2024

Reduced-Order Modeling of Indirect Fluidized-Bed Particle Receivers with Axial Dispersion

Keaton J. Brewster[1], Jesse R. Fosheim[2], Federico Municchi[1], Winfred J. Arthur-Arhin[1], and Gregory S. Jackson[1]*

[1] Department. of Mechanical Engineering, Colorado School of Mines, Golden, CO, USA

[2] Brayton Energy LLC, Hampton, NH, USA

*Correspondence: Dr. Gregory S. Jackson, email: gsjackso@mines.edu

Abstract. Oxide particles present a heat transfer and thermal energy storage (TES) media for next-generation concentrating solar power (CSP) plants where the high-temperature particle TES can provide dispatchable solar power [1]. Transferring heat to flowing particles can be a challenge and bubbling fluidization is a promising method for increased heat transfer between the oxide particles and confining walls. Using experimentally calibrated correlations for particle-wall heat transfer coefficients [2], this study explores in a quasi-1D model of a narrow-channel counterflow fluidized bed how the high heat transfer coefficients from bubbling fluidization enable cavity-based indirect particle receivers. Particle-wall heat transfer coefficients exceeding 800 W m^{-2} K^{-1} support angled solar fluxes > 200 kW m^{-2} from high normal fluxes > 1200 kW m^{-2} with wall temperatures < 1000 ˚C. Parametric studies identify how gas flows, solar fluxes, and receiver heights impact receiver solar efficiency for a CSP plant. These modeling studies provide a basis for the development of an indirect narrow-channel fluidized particle receiver that has the potential to operate at normal solar fluxes over 1000 kW m^{-2} and solar efficiencies above 85%.

Keywords: Bubbling Fluidization, Fluidized Bed, Particle-Wall Heat Transfer, Particle Receivers

1. Introduction

Development of high temperature particle receivers is essential for coupling particle-based TES to modern CSP plants. The most heavily explored receiver technology in this field is the falling curtain particle receiver, being studied and tested globally [3]. This technology boasts potential high (>85%) thermal efficiencies and low capital cost, yet suffers from particle attrition with smaller diameters, and requires more expensive engineered absorptive particles. Recent progress in heat transfer in fluidized beds has garnered attention for indirect receiver options, which can achieve similarly high efficiencies, operate with any particle type, and offer the modularity to incorporate thermochemical energy storage. Specifically, the DOE has recently chosen to fund an NREL-led project studying a Light Trapping Particle Cavity Receiver (LTPCR), which employs a fluidized bed to increase particle-wall heat transfer. Mild bubbling fluidization has been shown to increase local particle-wall heat transfer coefficients by 400% compared to a non-fluidized condition [2], [4]. This increased particle-wall heat transfer allows for effective solar fluxes up to 300 kW m^{-2} while keeping the enclosing walls below 1000 ˚C. Higher allowable solar fluxes proportionally decrease the required receiver size and initial capital cost of operation.

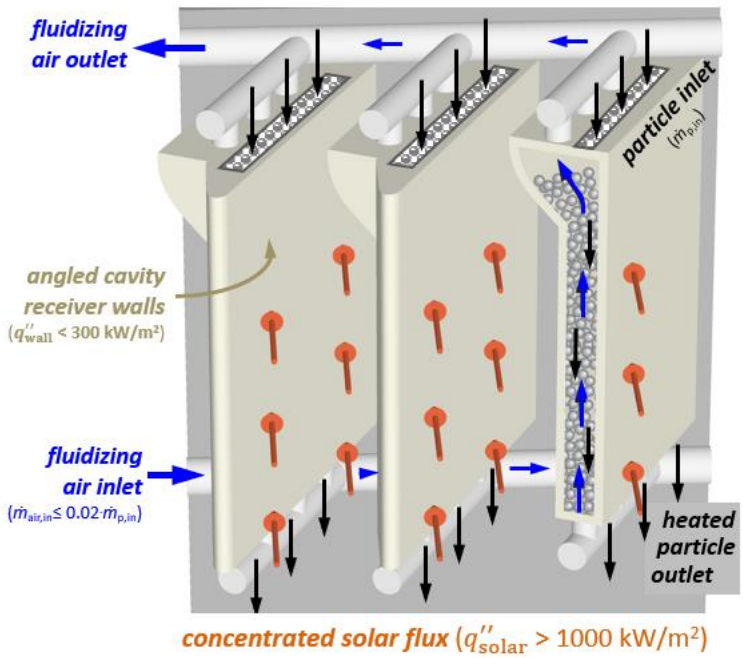

Figure 1. *Generalized indirect fluidized bed particle receiver design, with incident solar fluxes of up to 300 kW m^{-2}, a downward dense flow of particles (ϕ_p > 0.4), and a small upward velocity of fluidizing gas ($\dot{m}_g$ / $\dot{m}_p$ < 0.02). Image credit Dr. Robert Kee*

Mild bubbling fluidization has a mechanism for increased heat transfer has been studied largely in the context of particle heat exchangers [4], [5]. Different fluidized bed receiver configurations have also been considered [6], [7], [8]. It has also been employed as a heat transfer mechanism for REDOX cycles and other applications in chemical engineering [9], [10]. Fluidization greatly increases convective heat transfer between the walls and particles, often by a factor of ~400% depending on the particle type [4], [11], [12]. Tubular solar receivers, which employ fluidized olivine sand(d_p = 30 μm), have achieved heat transfer coefficients as high as 1200 +/- 400 W m^{-2} K^{-1} [13]. Narrow channel fluidized beds offer pathways to high heat transfer coefficients with CARBO HSP ($h_{T,w}$ > 800 W m^{-2} K^{-1}) with very small gas to particle mass flux ratios ($\dot{m}_g$ / $\dot{m}_p$ < 1%). Using smaller particles in such a configuration may provide a pathway to further increased heat transfer. In the context of heat exchangers, the primary benefit of an increased heat transfer coefficient is a smaller required heat exchanger size to extract the same amount of thermal energy. For a receiver, the benefit is the same, with the additional benefit of reduced wall temperatures. If particle temperatures > 700 ˚C leaving the receiver are to be achieved, then wall temperatures are going to be even higher. Increased heat transfer coefficients above 800 W m^{-2} K^{-1} allow for direct wall fluxes up to 200 kW m^{-2} and wall temperatures < 1000 ˚C. This paper explores the effects of different parameters such as gas flow rates, solar fluxes, and receiver heights for narrow channel fluidized bed receivers and how they effect performance and feasibility.

2. Methodology

One large challenge with technologies that have yet to be tested at large scales is comprehensive analyses which are representative of physical trends, yet computationally inexpensive so wider parametric studies can be conducted. For this application, we have developed a robust reduced order model which is vertically discretized as seen in Figure 2 (a), and solves multi-phase mass, momentum, and energy balances. This model is adapted from a Fluidized Bed Heat Exchanger (FBHX) model described by Foshiem et al [4], and is numerically solved using iterative multi-equation solvers in MATLAB [14]. Thermodynamic properties are evaluated using the MATLAB [14] interface for Cantera [15], which uses publicly available properties for air, and NASA9 polynomial fits for particle properties, with data

published by Georgia Tech [16]. The receiver modeled is a generic design(Figure 2(b)) which does not account for edge effects and uses the entire length (Δx_w) as a single node. This design uses angled solar fluxes (equivalent to angled receiver walls) to reduce effective solar fluxes down from 1000 to 200 kW m^{-2}, as was similarly used in the DOE sponsored ELEMENTS[10] and LTPCR [17], [18] projects.

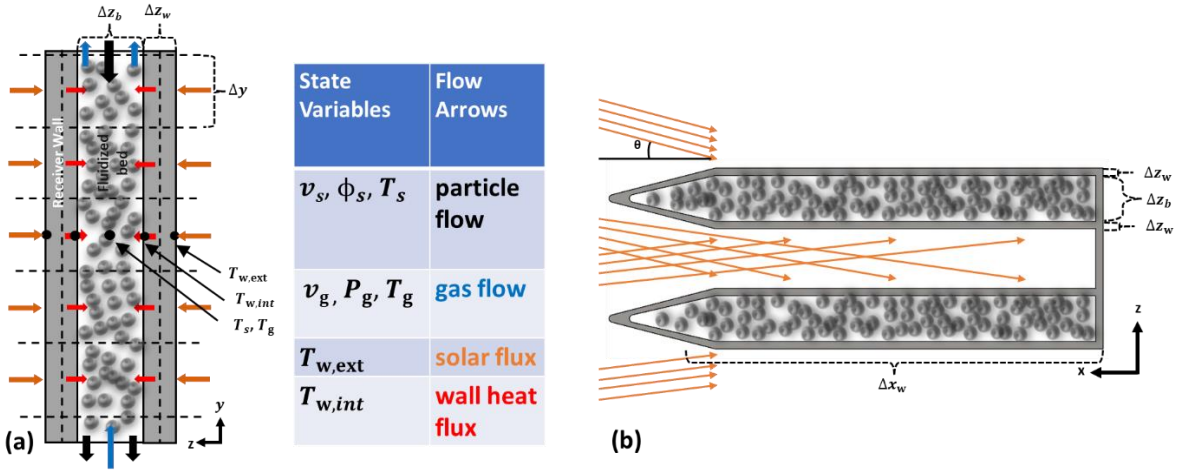

Figure 2. (a) *Model discretizations and flow diagram for the modeled indirect fluidized bed particle receiver.* ***(b)*** *Schematic of receiver cross-section highlighting the flux spreading and light trapping capabilities of this generalized design.*

To achieve physical results with a reduced order model, we used several experimentally calibrated correlations for particle-wall heat transfer, $h_{T,w}$, axial dispersion, D_{yy}, and interphase heat transfer $h_{T,g\text{-}s}$. One of the most critical parameters in indirect receivers is $h_{T,w}$, which dictates the maximum allowable heat flux through the receiver for the allowed enclosure temperature. The empirical correlation uses here relies on experimental data [2], and uses the following definitions of the heat transfer coefficient:

$$h_{T,w} = h_{T,w,pc} + h_{T,w,rad} \tag{1}$$

Where the radiative component is calculated assuming gray surfaces and view factors of one [19]:

$$h_{T,w,rad} = \sigma\left(T_s^2 + T_{w,int}^2\right)/(\epsilon_s^{-1} + \epsilon_w^{-1} - 1) \tag{2}$$

The convective component is captured via a Nusselt number which is discussed in the next section.

$$h_{T,w,pc} = \left(Nu_{pc}\lambda_g\right)/d_p \tag{3}$$

Another critical empirical parameter is axial particle mixing, which is captured in the solid phase energy balance via a dispersion coefficient. A derivation of how this coefficient was calculated and fit is included in the following section. This dispersion term captures particles which rise and fall in the bed due to bubbles transporting particles. This behavior is captured through a diffusive flux term as follows:

$$\dot{q}''_{s,disp} = D_{yy,s}\phi_s\rho_s c_{p,s}\frac{dT_s}{dy} \tag{4}$$

The internal fluidized bed conservation equations for the gas and solid phases for momentum, mass, and gas energy balances are as described by Foshiem et. al [4]. The solid

phase energy balance is also similar, but includes the addition of axial dispersion, creating the following equation:

$$\frac{\partial}{\partial y}(\phi_s \rho_s u_s h_s) = h_{\mathrm{T,g-s}}\rho_{\mathrm{A,g-s}}(T_\mathrm{s} - T_\mathrm{g}) + h_{\mathrm{T,w}}\rho_{\mathrm{A,w}}(T_\mathrm{w} - T_\mathrm{s}) + \frac{\partial}{\partial y}\left(\lambda_\mathrm{s}\frac{\partial T_\mathrm{s}}{\partial y}\right) + \frac{\partial}{\partial y}\left(D_{\mathrm{yy,s}}\phi_\mathrm{s}\rho_\mathrm{s}c_{p,\mathrm{s}}\frac{\partial T_\mathrm{s}}{\partial y}\right) \quad (5)$$

Rather than using sCO2 channels as done in Foshiem et al's FBHX model, this model is adapted to capture external radiative balances. The residual for external wall node energy balances equates input radiation, re-radiation, external convective losses due to natural convection to the ambient, and conduction in the *z* and y directions. The external wall energy balance becomes:

$$\alpha_\mathrm{w}A_\mathrm{z}\dot{q}''_{\mathrm{sol,eff}} - \epsilon_\mathrm{w}A_\mathrm{z}F_\mathrm{amb}\sigma\left(T^4_{\mathrm{w,ext}} - T^4_\mathrm{amb}\right) + h_{\mathrm{conv,ext}}A_\mathrm{z}\left(T_\mathrm{amb} - T_{\mathrm{w,ext}}\right) + \frac{\lambda_\mathrm{w}A_z}{\Delta z}\left(T_{\mathrm{w,ext}} - T_{\mathrm{w,int}}\right) + \frac{\lambda_\mathrm{w}A_y}{\Delta y}\left(T_{\mathrm{w,ext},y} - T_{\mathrm{w,ext},y-\Delta y}\right) = 0 \quad (6)$$

The view factor F_amb from the external walls to the ambient will vary based on the receiver geometry, but for a 0.1 m length in x and 0.0176 m between the fins gives F_amb = 0.08 [20]. This assumes the virtual surface is at a right angle at the edge of the channel. Any radiation that hits the base of the channel at x = 0 is assumed to stay within the system. The distance between the fins is the minimum distance for a 0.1 m fin that allows light to cover the entire surface for $\theta = 10°$. Edge effects are not considered in this model. The receiver walls are set as SS316, and the external surface is modeled as being coated with the highly absorptive Pyromark 2500 [21].

For the internal wall nodes, we equate the conduction in the z and y directions to the heat transfer into the bed.

$$\frac{\lambda_\mathrm{w}A_z}{\Delta z}\left(T_{\mathrm{w,ext}} - T_{\mathrm{w,int}}\right) + \frac{\lambda_\mathrm{w}A_y}{\Delta y}\left(T_{\mathrm{w,int},y} - T_{\mathrm{w,int},y-\Delta y}\right) + h_{\mathrm{T,w}}A_y\left(T_\mathrm{s} - T_{\mathrm{w,int}}\right) = 0 \quad (7)$$

Mass and momentum balances are only performed in the fluidized bed and are identical to those used in Foshiem et al's study on fluidized bed heat exchangers [4].

3. Experimental Methods

A robust fluidized bed heat transfer test facility has been assembled and used to measure $h_{\mathrm{T.w}}$ at temperatures up to 450 ˚C, varied particle types < 410 µm, and fluidizing gas velocities up to 0.4 m s^{-1}. This test facility offers a 0.012 x 0.1 m cross sectional area and 0.4 m height. This system can well approximate a single channel of a fluidized bed heat exchanger (FBHX) or indirect particle receiver. Extensive measurements in this test facility have allowed for empirical additions to this reduced order model to allow for reliable results and minimal computational time.

Experimental efforts here at mines have led to the development of a robust Nusselt number correlation which is used to predict particle-wall heat transfer coefficients as a function of excess dimensionless gas velocity, $\widehat{U}$, and the laminar Archimedes number, *Al*. These efforts capture impacts of gas velocities up to 0.4 m s^{-1} and particle types for particles under consideration for use in thermal energy storage (TES). Temperature dependencies were experimentally measured up to 450 ˚C and are well characterized by the increase in air conductivity with temperature, which has been well established for temperatures under consideration for indirect receivers. These data, in addition to other sets with alternate particle types and operating conditions, are discussed in further detail in Brewster et. al [2]. The Nusselt

correlation captures dependencies via the laminar Archimedes number, *Al,* excess fluidization velocity, $\widehat{U}$, and the two-phase bed Prandtl number. This approach follows a similar study by Molerus [11], [12].

$$Nu_{\mathrm{pc}}(1+Pr^{-1}) = f(Al)f\left(\widehat{U}\right) \tag{8}$$

Where these dimensionless groups are defined as:

$$Al = \sqrt{d_{\mathrm{p}}^3 g}\left(\rho_{\mathrm{s}}-\rho_{\mathrm{g}}\right)/\mu_{\mathrm{g}} \tag{9}$$

$$Pr = \left(2c_{p,\mathrm{s}}\mu_{\mathrm{g}}\right)/\lambda_{\mathrm{g}} \tag{10}$$

$$\widehat{U} = \left(U_{\mathrm{g}}-U_{\mathrm{mf}}\right)\left(\rho_{\mathrm{s}}c_{p,\mathrm{s}}/\lambda_{\mathrm{g}}g\right)^{1/3} \tag{11}$$

The *Al* and $\widehat{U}$ dependences are captured as:

$$f(Al) = \begin{cases} 0.129Al^{0.594} & Al \le 1500 \\ 2.089Al^{0.174} & Al > 1500 \end{cases} \tag{12}$$

$$f\left(\widehat{U}\right) = \begin{cases} 0.241 + 0.043\widehat{U}^{0.905}\exp\left(-\widehat{U}/71.673\right) & \widehat{U} \ge 0 \\ 0.241 & \widehat{U} < 0 \end{cases} \tag{13}$$

While $h_{\mathrm{T,w}}$ is a critical empirical component of this presented reduced order model, another critical component is the impacts of axial dispersion, D_{yy}, on receiver performance. Axial dispersion takes place when fluidizing gas lifts and redistributes particles as they fall through the receiver. This behavior is highly beneficial for increasing particle-wall heat transfer but has non-intended effects on vertical temperature profiles. In our lab scale rig, pressures are measured at several different vertical locations, and the pressure gradient in the gas is driven by particle-gas drag forces. A full derivation of these trends is beyond the scope of this paper, but temporal fluctuations in particle velocity can be extracted from temporal variations in the pressure gradient, allowing us to calculate this dispersion coefficient which is generically defined as [22]:

$$\begin{aligned} D_{\mathrm{yy,s}} &= \frac{1}{2\Delta t}\left[\left(y_{\mathrm{s}}(t)-y_{\mathrm{s}}(t-\Delta t)\right)\right]^2 \approx \frac{\Delta t}{2}\left[\left(u_{\mathrm{y,s}}-u_{\mathrm{y,g}}\right)'\right]^2 \\ &\approx \frac{D_h}{2u_{mf}}\left(\frac{d\beta_{drag}}{d\left(u_{y,s}-u_{y,g}\right)}\right)^{-1}\left(\phi_s\frac{dp}{dy}\right)' \end{aligned} \tag{14}$$

where Δt is a time constant associated with the solid velocity fluctuations and y_{s} is the mean solid particle displacement. The far right-hand-side replaces the displacement with the $\Delta t\left(u_{\mathrm{y,s}}-u_{\mathrm{y,g}}\right)'$ and thereby provides an approach to relating experimentally measurable quantities in eq. 1 such as pressure p and ϕ_{s} to $D_{\mathrm{yy,s}}$. Using this method for calculating the dispersion coefficient, we can also define a characteristic Peclet number as:

$$Pe_{\mathrm{y,s}} = \frac{D_{\mathrm{h}}\left(U_{\mathrm{g}}-U_{\mathrm{mf}}\right)}{D_{\mathrm{yy,s}}} = 3.92\ [-] \tag{15}$$

As is often done, we approximate these trends to have a constant Peclét number, which with this dataset was calibrated to be 3.92, similar to values reported for comparable systems [23], [24]. The use of these empirical correlations for axial dispersion and particle-wall heat

transfer allows us to employ the previously described model over a wide range of conditions with a minimal computational load.

4. Results and Discussion

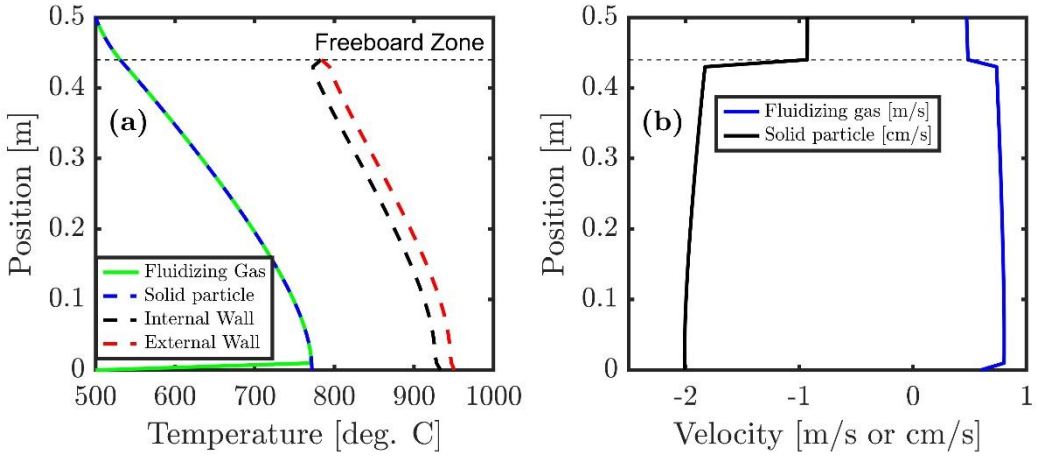

Figure 3. *Model solution at base condition ($\dot{m}''_p$ = 20 kg m^{-2} s^{-1}, $\dot{m}''_g$ = 0.15 kg m^{-2} s^{-1}) displaying (a) temperature profiles and (b) velocity profiles. This case achieves a solar efficiency, η_{sol} of 85% with maximum wall temperatures below 1000 ºC, at an excess dimensionless gas velocity, $\hat{U}$, of 53. This is accomplished with a low gas to particle flow ratio of 0.4%, indicating minimal thermal losses from the fluidizing gas.*

The primary aim of this reduced order model is to construct broad trends for fluidized bed receiver applications and identify feasibility of this technology at scale. Our base case, as displayed in Figure 3, runs for a 0.5 m tall receiver with 500 ˚C particle and gas inlet temperatures, an effective solar flux of 200 kW m^{-2}, and uses 408 µm CARBO HSP 40/70 particles as were tested experimentally. These conditions were chosen to represent a general geometry considered for different indirect fluidized bed receiver prototypes and achieves particle outlet temperatures above 720 ˚C as is desired for high temperature Brayton power cycles being considered. This base case alone also achieves highly desirable metrics such as solar efficiencies above 85%, which are comparable to falling curtain particle receivers, and wall temperatures below 1000 ˚C, which for this given solar flux would not be possible without bubbling fluidization.

One uncertainty in fluidized bed receiver design is identifying design conditions for particle and gas flow rates through the receiver. As the fluidizing gas velocity increases, the particle-wall heat transfer coefficient increases rapidly and then flattens out. Providing excessively high fluidization velocities not only has minimal heat transfer benefits but starts to increase parasitic thermal losses from the fluidizing gas and can begin to introduce flow instabilities as the particle-gas drag force will eventually begin to pneumatically lift particles. These trade-offs are readily observed in Figure 4 (a) and (c), where increases in gas velocity decrease the outer wall temperature yet have diminishing benefits beyond a gas mass flux of 0.1 kg m^{-2} s^{-1}, or a $\hat{U}$ of approximately 25. The conditions tested are given in Table 1., with the varied parameters in this study being gas mass flux, total receiver height, and solar flux.

Table 1. *Reduced order model parameters.*

Parameter	Symbol	Values	Units
Particle Inlet Temperature	$T_{p,in}$	500	°C
Gas Inlet temperature	$T_{g,in}$	500	°C
Effective solar flux	$\dot{q}''_{sol}$	100-400	kW m^{-2}
Particle Mass Flux	$\dot{m}''_{p}$	20	kg m^{-2} s^{-1}
Gas Mass Flux	$\dot{m}''_{g}$	0.05-0.25	kg m^{-2} s^{-1}
Receiver Height	y_{rec}	0.2-4	m
Receiver width	x_b	0.1	m
Receiver depth	z_b	0.012	m
Freeboard zone height	y_{fb}	0.065	m
Freeboard zone depth	z_{fb}	0.020	m
Solar absorptivity	α_w	0.95	-
IR emissivity	ε_w	0.78	-
Ext. wall view factor to ambient	F_{amb}	0.08	-
Particle mean diameter	d_p	408	μm
Particle density	ρ_s	3620	kg m^{-3}

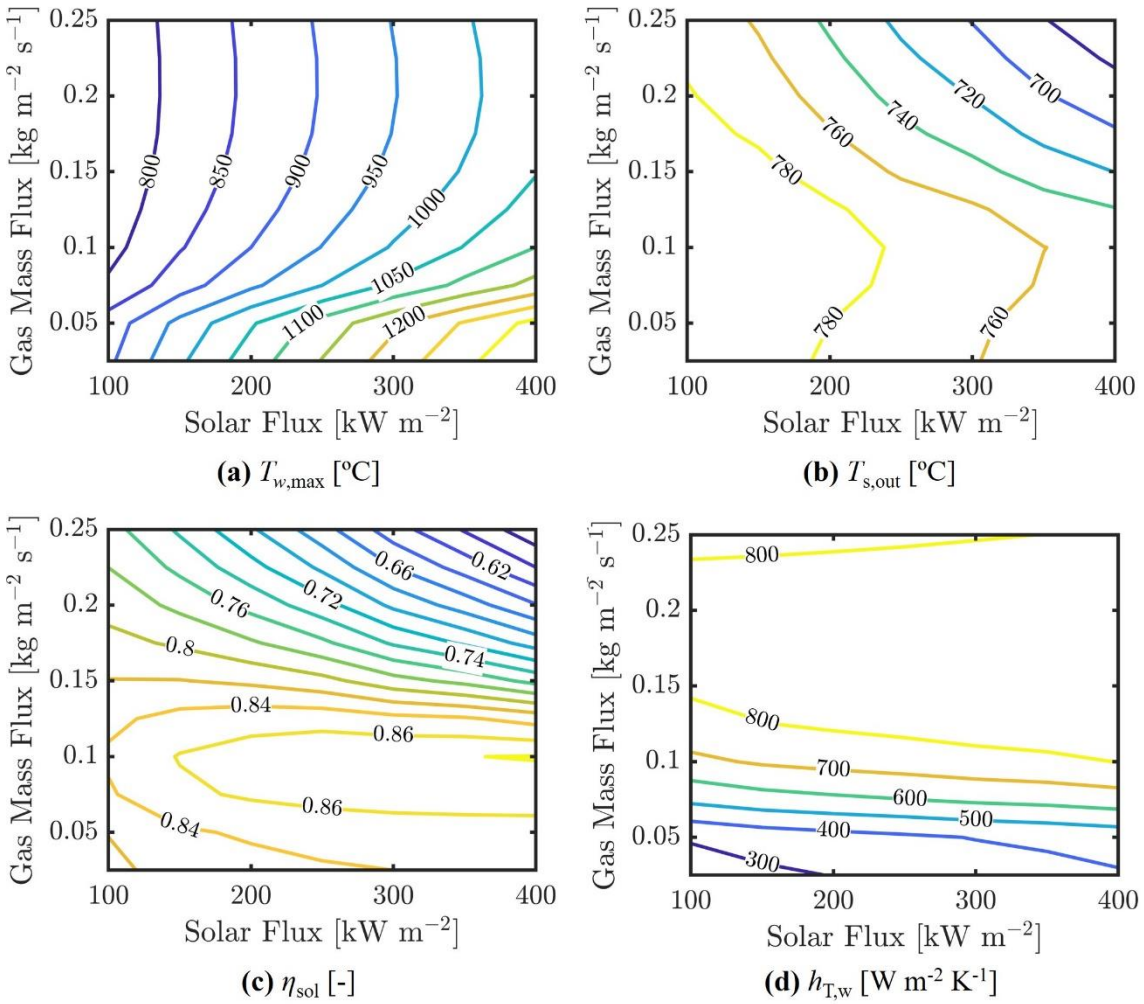

Figure 4. *Parametric studies varying gas mass fluxes and solar flux concentrations with a fixed total input power. (a) Maximum external wall temperatures (b) particle outlet temperatures, (c) thermal efficiency, and (d) particle-wall heat transfer coefficients. This study shows that the introduction of mild fluidization can significantly decrease external wall temperatures for a given flux, allowing for decreased total receiver size for a given thermal load.*

While Figure 3 showed that our base case can achieve the desired performance characteristics for a receiver, the primary benefit of introducing mild bubbling fluidization in a receiver is the increased allowable solar flux incident on the walls while maintaining mechanically stable external wall temperatures. To explore this benefit, which arises from the increase in $h_{T,w}$ of approximately 400% compared to a non-fluidized condition, we conducted a study where we varied both the gas mass flux and the solar flux, where the receiver size was varied to keep a constant total thermal load, and by extension relatively constant particle outlet temperature. This displayed the trend of enhanced allowable flux clearest in Figure 4(a), where the max wall temperature contour at 1000 ˚C lies at nearly 150 kW m^{-2} near the x-axis, which is at a non-fluidized condition, as compared to a high flux above 300 kW m^{-2} when the bed is well fluidized at a gas mass flux of 0.15 kg m^{-2} s^{-1}. This increase in allowable flux corresponds to a smaller receiver size, which can decrease total receiver cost as well as reduce the area available for convective and re-radiation losses. This shorter receiver with high fluxes achieves thermal efficiencies above 85% in Figure 4 (c), reaching the desired metric of above 85%. It should be noted that the displayed efficiencies here are optimistic because they do not directly account for vertical conductive losses in the walls to the receiver structure, nor do they account for any transience, which is always present in CSP systems. Some of these metrics are also a function of the specific design, which will see non-constant solar fluxes and have slightly different light capturing capabilities depending on the geometry.

5. Conclusions

Parametric modeling cases have shown that indirect fluidized bed particle receivers can produce particle outlet temperatures above 700 ˚C under effective solar fluxes of 200 kW m^{-2} and thermal efficiencies above 85%. These high performances are made possible through increased particle-wall heat transfer from mild bubbling fluidization with gas mass flow rates often under 1% of particle mass flow rates. A parametric study identified the capability of mild bubbling fluidization to increase effective solar fluxes from 150 to 300 kW m^{-2} while achieving target particle outlet temperatures > 720 ˚C and wall temperatures < 1000 ˚C. The resulting decrease in total receiver size can help decrease receiver CAPEX costs and suggests scale-up feasibility of indirect fluidized bed particle receivers. This technology is currently in a prototyping phase, with multiple smaller scale projects previously testing fluidized bed heat transfer [2], [7] and new projects exploring larger scale prototyping. The US DOE funded Light Trapping Particle Cavity Receiver (LTPCR) project, led by Dr. Zhiwen Ma of the national renewable energy laboratory, is currently beginning to manufacture a 100 kW_{th} fluidized bed receiver with enhanced light trapping capabilities which will be tested at KSU in Saudi Arabia. This work and related efforts have shown that indirect particle receivers are capable, and these scale-up efforts will provide further design insights into commercialization.

Data availability statement

The data will be made available upon request to the corresponding author.

Author contributions

Keaton J. Brewster: Methodology, Software, Writing – Original draft preparation. **Jesse R. Fosheim**: Software, Writing – Proofing. **Federico S. Municchi**: Methodology, Writing – Proofing. **Winfred R. Arthur-Arhin:** Software, Writing – Proofing. **Gregory S. Jackson:** Conceptualization of this study, Methodology, Writing – Original draft preparation.

Competing interests

The authors declare that they have no competing interests.

Funding

This work was performed under grants from the U.S. Department of Energy Solar Energy Technology Office under award numbers DE-EE0008538 and DE-EE0009812 (Shane Powers and Dr. Rajgopal Vijaykumar, program managers) and with funding from the Alliance for Sustainable Energy, LLC, Managing and Operating Contractor for the National Renewable Energy Laboratory for the U.S. Department of Energy. This material is

based upon work supported by the National Science Foundation Graduate Research Fellowship under Grant No. DGE-2137099.

Acknowledgements

The authors acknowledge the support from other members of our lab at the Colorado School of Mines including Dr. Fuqiong Lei, Yahya Bokhary, Dr. Wanjun Dang, and Xavier Hernandez. We would also like to acknowledge our collaborator Dr. Zhiwen Ma of the National Renewable Energy Laboratory.

References

[1] M. Mehos *et al.*, “Concentrating Solar Power Gen3 Demonstration Roadmap,” NREL/TP--5500-67464, 1338899, Jan. 2017. doi: 10.2172/1338899.

[2] K. J. Brewster *et al.*, “Particle-wall heat transfer in narrow-channel bubbling fluidized beds for thermal energy storage,” *Int. J. Heat Mass Transf.*, vol. 224, p. 125276, Jun. 2024, doi: 10.1016/j.ijheatmasstransfer.2024.125276.

[3] C. K. Ho, “A review of high-temperature particle receivers for concentrating solar power,” *Appl. Therm. Eng.*, vol. 109, pp. 958–969, Oct. 2016, doi: 10.1016/j.applthermaleng.2016.04.103.

[4] J. R. Fosheim, X. Hernandez, J. Abraham, A. Thompson, B. Jesteadt, and G. S. Jackson, “Narrow-channel fluidized beds for particle-sCO2 heat exchangers in next generation CPS plants,” *AIP Conf. Proc.*, vol. 2445, no. 1, p. 160007, May 2022, doi: 10.1063/5.0085934.

[5] W. Arthur-Arhin *et al.*, “Testing of a 40-kWth Counterflow Particle-Supercritical Carbon Dioxide Narrow-Channel, Fluidized Bed Heat Exchanger,” *SolarPACES Conf. Proc.*, vol. 1, Feb. 2024, doi: 10.52825/solarpaces.v1i.634.

[6] J. Martinek and Z. Ma, “Granular Flow and Heat-Transfer Study in a Near-Blackbody Enclosed Particle Receiver,” *J. Sol. Energy Eng.*, vol. 137, no. 5, p. 051008, Oct. 2015, doi: 10.1115/1.4030970.

[7] D. C. Miller, C. J. Pfutzner, and G. S. Jackson, “Heat transfer in counterflow fluidized bed of oxide particles for thermal energy storage,” *Int. J. Heat Mass Transf.*, vol. 126, pp. 730–745, 2018, doi: https://doi.org/10.1016/j.ijheatmasstransfer.2018.05.165.

[8] K. Jiang, X. Du, Q. Zhang, Y. Kong, C. Xu, and X. Ju, “Review on gas-solid fluidized bed particle solar receivers applied in concentrated solar applications: Materials, configurations and methodologies,” *Renew. Sustain. Energy Rev.*, vol. 150, p. 111479, 2021, doi: https://doi.org/10.1016/j.rser.2021.111479.

[9] L. Imponenti, K. J. Albrecht, R. Kharait, M. D. Sanders, and G. S. Jackson, “Redox cycles with doped calcium manganites for thermochemical energy storage to 1000 °C,” *Appl. Energy*, vol. 230, pp. 1–18, Nov. 2018, doi: 10.1016/j.apenergy.2018.08.044.

[10] G. S. Jackson *et al.*, “CSP ELEMENTS: High-Temperature Thermochemical Storage with Redox-Stable Perovskites for Concentrating Solar Power,” Colorado School of Mines,

Golden, CO (United States), DOE-CSM-6537, Nov. 2016. Accessed: Oct. 07, 2023. [Online]. Available: https://www.osti.gov/biblio/1333903

[11] O. Molerus, “Heat transfer in gas fluidized beds part 1.,” *Powder Technol.*, vol. 70, no. 1, pp. 1–14, Apr. 1992, doi: 10.1016/0032-5910(92)85048-Z.

[12] O. Molerus, “Heat transfer in gas fluidized beds part 2. Dependence of heat transfer on gas velocity,” *Powder Technol.*, vol. 70, pp. 15–20, 1992.

[13] A. Le Gal *et al.*, “Thermal analysis of fluidized particle flows in a finned tube solar receiver,” *Sol. Energy*, vol. 191, pp. 19–33, Oct. 2019, doi: 10.1016/j.solener.2019.08.062.

[14] Mathworks, “MATLAB version 23.2.0.2365128 (R2023b).” The Mathworks, Inc., Natick, Massachusetts, 2023. [Online]. Available: www.mathworks.com

[15] D. G. Goodwin, H. K. Moffat, I. Schoegl, R. L. Speth, and B. W. Weber, “Cantera: An Object-oriented Software Toolkit for Chemical Kinetics, Thermodynamics, and Transport Processes.” 2022. doi: 10.5281/zenodo.6387882.

[16] B. K. Arkhurst, S. A. Brankovic, and others, “Thermophysical Properties Database of Gen3 CSP Materials.” Accessed: Mar. 09, 2023. [Online]. Available: https://gen3csp.gatech.edu/

[17] M. Carter, D. Korba, J. Martinek, Z. Ma, and L. Li, “Thermomechanical Stress and Creep-Fatigue Analysis of a High-Temperature Prototype Receiver for Heating Particles,” presented at the ASME 2023 17th International Conference on Energy Sustainability collocated with the ASME 2023 Heat Transfer Summer Conference, American Society of Mechanical Engineers Digital Collection, Sep. 2023. doi: 10.1115/ES2023-107262.

[18] K. Appaswamy, J. Schirck, C. Punchi Wedikkara, A. Morris, and Z. Ma, “Multiphase Modeling in a Parallel Plate Fluidized Bed Receiver for Concentrating Solar Power,” presented at the ASME 2023 17th International Conference on Energy Sustainability collocated with the ASME 2023 Heat Transfer Summer Conference, American Society of Mechanical Engineers Digital Collection, Sep. 2023. doi: 10.1115/ES2023-106824.

[19] M. Eriksson and M. R. Golriz, “Radiation heat transfer in circulating fluidized bed combustors,” *Int. J. Therm. Sci.*, vol. 44, no. 4, pp. 399–409, Apr. 2005, doi: 10.1016/j.ijthermalsci.2004.11.006.

[20] M. F. Modest, *Radiative Heat Transfer*. McGraw Hill, 1993.

[21] C. K. Ho, A. R. Mahoney, A. Ambrosini, M. Bencomo, A. Hall, and T. N. Lambert, “Characterization of Pyromark 2500 Paint for High-Temperature Solar Receivers,” *J. Sol. Energy Eng.*, vol. 136, no. 1, p. 014502, Feb. 2014, doi: 10.1115/1.4024031.

[22] A. J. Banko and J. K. Eaton, “Particle dispersion and preferential concentration in particle-laden turbulence,” in *Modeling Approaches and Computational Methods for Particle-Laden Turbulent Flows*, Elsevier, 2023, pp. 43–79. doi: 10.1016/B978-0-32-390133-8.00011-6.

[23] N. Mostoufi and J. Chaouki, “Local solid mixing in gas–solid fluidized beds,” *Powder Technol.*, vol. 114, no. 1–3, pp. 23–31, Jan. 2001, doi: 10.1016/S0032-5910(00)00258-8.

[24] R. W. Breault, “A review of gas–solid dispersion and mass transfer coefficient correlations in circulating fluidized beds,” *Powder Technol.*, vol. 163, no. 1, pp. 9–17, 2006, doi: https://doi.org/10.1016/j.powtec.2006.01.009.